

Designing Novel Nonsymmetric Ag/AgI Nanoplates for Superior Photocatalytic Activity

Misbah Ullah Khan, Hongjun You,* Xiaotong Liu, Lingling Zhang, and Jixiang Fang*

Precisely engineering the decoration of metal nanoparticles on the special surface of semiconductor represents a promising strategy to design efficient metal–semiconductor heterostructured photocatalysts. This study demonstrates a versatile soft-template method to fabricate a novel nonsymmetrical heterostructured Ag/AgI nanoplate, in which only one side surface of the nanoplate is covered with uniform 2D Ag nanoweb. Compared with symmetrical heterostructure, the nonsymmetrical heterostructure may further facilitate the separation of photogenerated electron–hole pairs and shows a greatly enhanced photocatalytic activity. This study may open up a new way to improve the photocatalytic property by synthesizing nonsymmetrical metal–semiconductor composites.

As efficient photocatalysts, various semiconductors and their compounds have attracted great interests in wide application fields, such as the environmental remediation, energy production and conversion, and biological and biomedical sensing.^[1–4] Shortening the travel distance of photogenerated carriers migrating from the inner of the semiconductor to the surface can effectively prevent the recombination of electron–hole pairs during the photocatalyst process.^[5–9] Up to now, various morphologies and structures, such as nanocubes, nanospheres, nanowires, nanobelts, nanoprisms, and hollow or porous nanostructures, have been synthesized to improve the photocatalytic property.^[10–12] Specially, constructing heterojunctions by combining semiconductors with noble metals or metal oxides has been proved to be a very effective approach to prevent the recombination of electron–hole pairs.^[10–16]

As shown in **Figure 1A**, due to the Schottky effect formed at the interface of semiconductor and metal, an internal electric field is produced that can facilitate the separation of electron–hole pairs and induce faster carrier migration.^[1–4,17,18] The photogenerated electrons will be trapped by the metal to catalyze the reducing reaction. The holes remained on the semiconductor surface to catalyze the oxidation reaction.^[1–4,19,20]


However, if all the outside surface of semiconductor is decorated with metal nanoparticles (NPs), the actual photocatalytic activity will be limited. As, in this situation, the electrons will migrate to the metal NPs along the formed internal electric field and the holes will be suppressed by the electric field to remain in the interior of the semiconductor, as shown in **Figure 1B**. The inner holes not only cannot perform catalytic function for the oxidation reaction but also will combine with new produced electrons. An assumption suggested here is that if a special heterojunction can be created as shown in **Figure 1C**, the separation of electron–hole

pairs might be further improved. Unfortunately, at present, it is still a challenge for people to decorate the nanostructured semiconductor with metal NPs on partial selected surface to form the novel nanostructures.^[21–23]

Nanostructured silver halides (AgX, X = Cl, Br, I) and their hybrids have recently attracted great interest.^[13–16,24–27] They can be easily disintegrated to in situ generate metallic Ag on the AgX surface by microwave or UV light irradiation, which not only can facilitate the separation of electrons and holes, but can also greatly enhance the absorbance of light in the visible region and accordingly increase utilization of light in the photocatalyst reaction due to the surface plasmon resonance absorption of Ag metal.^[28–31] However, the in situ produced Ag NPs always distribute on the entire outside surface of the nanostructured AgX.^[32–34]

In order to realize the control for the metal NPs on the partial selected surface of semiconductor, in this work, a soft-template strategy is developed to obtain a nonsymmetric heterostructure on 2D Ag/AgI nanoplate. The concept of soft template to synthesize such asymmetric heterostructures is provoked from our previous work that using PEG (polyethylene glycol)–water as soft template, asymmetric Au nanoplate with one side surface smooth and the other side sunken was achieved.^[35] Here, a soft template formed by ethylene glycol (EG) and potassium iodide (KI) is exploited to synthesize the nonsymmetric Ag/AgI nanoplate. Ag NPs can be well controlled to grow on only one side surface of the nanoplate with very uniform porous-like nanostructure. The other side surface of the AgI nanoplate remains clean without Ag NP decoration. As shown in **Figure 1C**, this novel nonsymmetric metal–semiconductor heterostructure may overcome the drawback of conventional metal–semiconductor heterostructures that are shown in **Figure 1B**. When the nonsymmetric Ag/AgI nanoplate is irradiated by light, the photogenerated electrons will be trapped by the porous Ag on

M. U. Khan, Prof. H. J. You, X. T. Liu, L. L. Zhang, Prof. J. X. Fang
 Key Laboratory of Physical Electronics and Devices of Ministry of Education
 School of Electronic and Information Engineering
 Xi'an Jiaotong University
 Xi'an, Shaanxi 710049, China
 E-mail: hjyou@mail.xjtu.edu.cn; jxfang@mail.xjtu.edu.cn

 The ORCID identification number(s) for the author(s) of this article can be found under <https://doi.org/10.1002/sml.201702948>.

DOI: 10.1002/sml.201702948

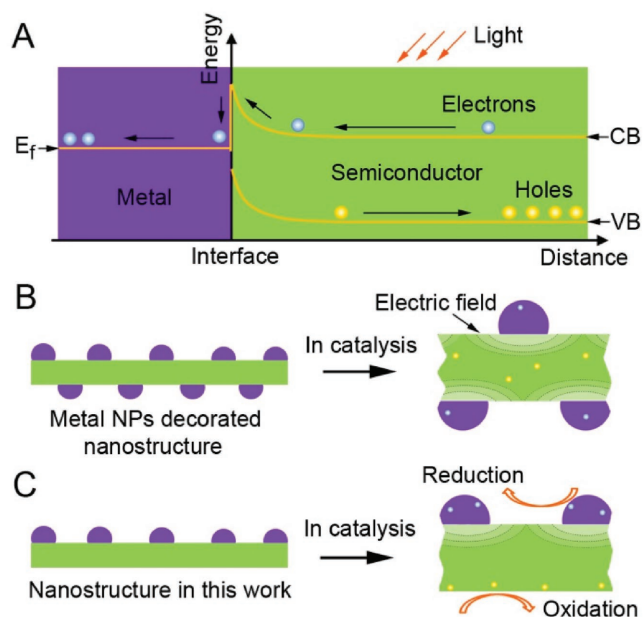


Figure 1. Schematic representation of photocatalytic mechanism for heterostructured metal-semiconductor nanocatalysts. A) Energy band structure at the Schottky barrier and electron-hole pair separation in the metal-semiconductor heterojunction. The photocatalytic mechanism for B) the nanostructure with the entire outside decorated with metal NPs and C) that only with one side decorated with metal NPs developed in this work.

the one side of the nanoplate to catalyst the reduction reaction. The holes will migrate along the electron field to the other side of the nanoplate to catalyst the oxidation reaction. Correspondingly, the photocatalytic activity should be greatly improved.

The one-pot synthesis for the Ag/AgI nanoplates is very simple but robust (see details in the Experimental Section and Figure S1, Supporting Information). EG and polyvinylpyrrolidone (PVP) are used as solution and surfactant, respectively. Silver acetate reacted with KI to form AgI precipitation. Just by increasing the silver acetate to excess compared with the quantity of KI, the nonsymmetric Ag/AgI nanoplates will be produced. When silver acetate is in deficiency, all of silver acetate reacts with KI and only forms pure AgI nanoplates. As shown by the scanning electron microscope (SEM) image in Figure 2A, the pure AgI nanoplates display hexagon shape with an average size of around 3 μm . It is noted that both side surfaces of the AgI nanoplate are smooth (Figure 2C). However, when KI is in deficiency, i.e., silver acetate is in excess, the redundant Ag ions may be reduced by the component of EG to produce Ag NPs on the surface of AgI nanoplates (i.e., formation of Ag/AgI nanoplates). The formation of Ag/AgI compound can be verified by the result of energy dispersive X-ray (EDX) analysis (Figure S2, Supporting Information). The atomic ratios of Ag and I are around 1:1 and 5:4 for AgI and Ag/AgI nanoplates, respectively. Unexpectedly, the Ag/AgI nanoplates display two kinds of surface morphologies, i.e., one is smooth and the other is rough, according to the SEM image in Figure 2B and Figure S3 (Supporting Information). The ratio of the amount for two kinds of surfaces is near 1:1. This result may indicate that the Ag/AgI nanoplates could be nonsymmetric morphology, in

which one side surface is smooth and the other side surface is rough (Figure 2D). The nonsymmetric morphology is further verified by the images from lateral view of the nanoplate (Figure 2D and Figure S4, Supporting Information). The thickness of the Ag/AgI nanoplates is around 20 nm. The small Ag NPs (around 10 nm) on the rough side connect together and hence form a 2D nanoweb (inset of Figure 2D). Unfortunately, under transmission electron microscope (TEM) observation, as shown in Figures S5 and S6 (Supporting Information), both AgI and Ag/AgI nanoplates are decomposed by electron beam irradiation. Thus, the high-resolution TEM images cannot be obtained to disclose the crystalline structure of AgI and Ag/AgI nanoplates.

The powder X-ray diffraction (PXRD) patterns of AgI nanoplates (Figure 3A) can be readily indexed to the planes of hexagonal AgI lattice (01-075-1528, JCPDS-ICDD). The PXRD patterns of Ag/AgI nanoplates can be indexed to two sets of crystal lattices. One set of relatively stronger diffraction pattern comes from the hexagonal AgI lattice (01-075-1528, JCPDS-ICDD), and the other set of relatively weaker diffraction pattern can be indexed to hexagonal close-packed (HCP) Ag lattice (00-041-1402, JCPDS-ICDD). The usual crystal structure of pure Ag is face-centered cubic lattice.^[36,37] The HCP Ag crystal can be obtained under some special conditions, such as the nanometer scale and surface effects.^[38,39] In the Ag/AgI nanoplates, the in situ grown Ag nanoweb on the one side will be influenced by the HCP nanocrystalline structure of AgI base, resulting in the formation of HCP Ag. The relative intensities of peaks are different for the AgI nanocrystal in AgI nanoplate and Ag/AgI nanoplate. This phenomenon could be determined by the stacking status of AgI nanoplate on the substrate for the PXRD. As shown in Figure S7 (Supporting Information), when AgI nanoplates are thickly loaded on the substrate, the (112) peak is the highest, and when AgI nanoplate are thinly loaded, the (110) peak becomes the highest and the (112) peak almost disappears. As explained with the schematic image in Figure S8A (Supporting Information), when a single AgI nanoplate is flatly loaded on the substrate, only (110) peak can be obtained in the PXRD pattern, similar to the report that only (110) peak is obtained in the PXRD pattern of rhombic dodecahedral Au nanocrystals.^[40] When AgI nanoplates are sloping on the substrate, the other peaks will appear, as shown in Figure S8B,C (Supporting Information).

The X-ray photoelectron spectra (XPS) of AgI nanoplates and Ag/AgI nanoplates are shown in Figure 3B–E. For I 3d_{5/2} and I 3d_{3/2}, the spectra of AgI nanoplates and Ag/AgI nanoplates are well coincident (Figure 3B), indicating that the elemental status of I is same. For Ag 3d_{5/2} and Ag 3d_{3/2}, the spectra peak of Ag/AgI nanoplates is obvious shift to a high value and become broader, compared with that of AgI nanoplates (Figure 3C). The Ag 3d_{5/2} and Ag 3d_{3/2} of AgI nanoplates lines appear at 367.7 and 373.7 eV (Figure 3D), indicating that Ag is present in the oxidation state. For the spectra of Ag/AgI, as shown in Figure 3E, the Ag 3d_{5/2} and Ag 3d_{3/2} peaks can be divided into Ag⁰ and Ag⁺ components. The peaks of Ag⁺ are higher than that of Ag⁰, consistent with EDX result, indicating that about 80% Ag atoms are in the AgI and 20% Ag atoms are in the pure Ag.

The morphology of AgI and Ag/AgI nanoplates shown in Figure 2 has been optimized by changing experimental

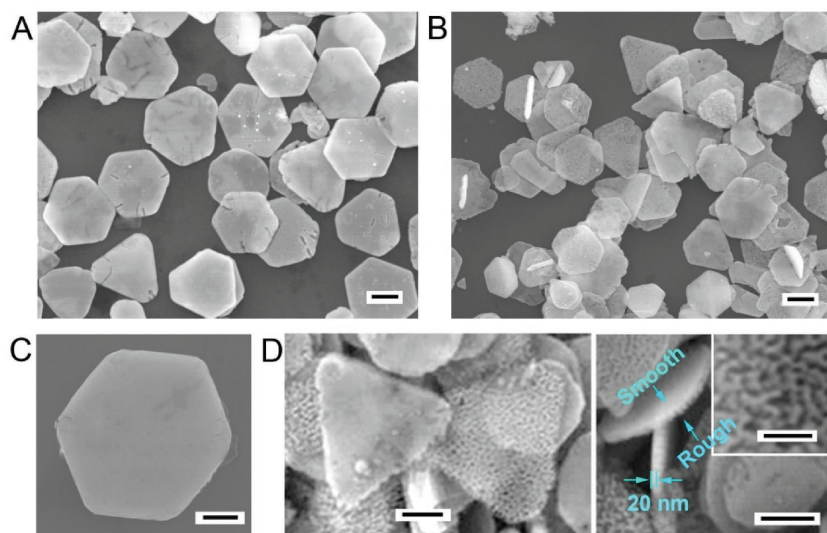


Figure 2. SEM images of AgI and Ag/AgI nanoplates. A) AgI nanoplates and B) Ag/AgI nanoplates in large area. C) Single AgI nanoplate with high magnification. D) Ag/AgI nanoplates with high magnification showing that one side is smooth and the other side is rough. The inset showing the rough structure on one side is very uniform. The scale bars in (A) and (B), (C) and (D), and the inset of (D) are 1 μm , 500 nm, and 100 nm, respectively.

conditions, such as the amount of EG and Ag precursor. Figure S9 (Supporting Information) shows the morphology transformation of AgI nanoplates synthesized with 2, 6, 9, and 12 mL EG. When EG is less than 9 mL, such as 2 and 6 mL, AgI particles with irregular shape are obtained (Figure S9A,B, Supporting Information). When EG is more than 9 mL, such as 12 mL, small and thick AgI nanoplate is produced. Figure S10 (Supporting Information) shows the SEM images of product synthesized with the concentrations of Ag precursor changing from 0.2×10^{-3} M to 2×10^{-3} M, 4×10^{-3} M, and 20×10^{-3} M.

Uniform AgI and Ag/AgI nanoplates can be formed only in a narrow window of experimental conditions. Various experimental conditions will change the kinetic process in the formation of the nanoplates.

The formation process of Ag/AgI nanoplates was investigated by the product obtained with different reaction times. At the very beginning of the reaction, there is almost no precipitation that can be collected from the synthesis solution. The SEM images of the products obtained with reaction times of 5, 10, 30, and 90 min are shown in Figure 4A. With the increase of reaction time, the morphology transforms from small NPs into porous nanoplates, nanoplates with smooth surfaces, and finally nanoplates with one side of rough surface.

The formation mechanism of Ag/AgI nanoplates was further studied with the density functional theory calculation (see details in the Supporting Information).^[41,42] The EG and KI are polar molecules. When they approach, their tips can be polarized from each other and the electrons-cloud will overlap to form hydrogen bonds (Figure 4B). The I atom in KI connects with hydroxyl groups in EG with -0.30 eV bond energy. The K atom in KI connects with oxygen atoms in EG with -0.51 eV bond energy. The I and K atoms each can connect with 2 EG molecules. The hydrogen bonds formed between KI and EG molecules locate in a 2D plane. When enough of KI and EG molecules connect together, 2D EG–KI soft templates will be formed in the synthesis solution, as shown in Figure 4C. This situation is similar to the 2D water-PEG soft template in our recent work in which Au nanoplates have been synthesized.^[35]

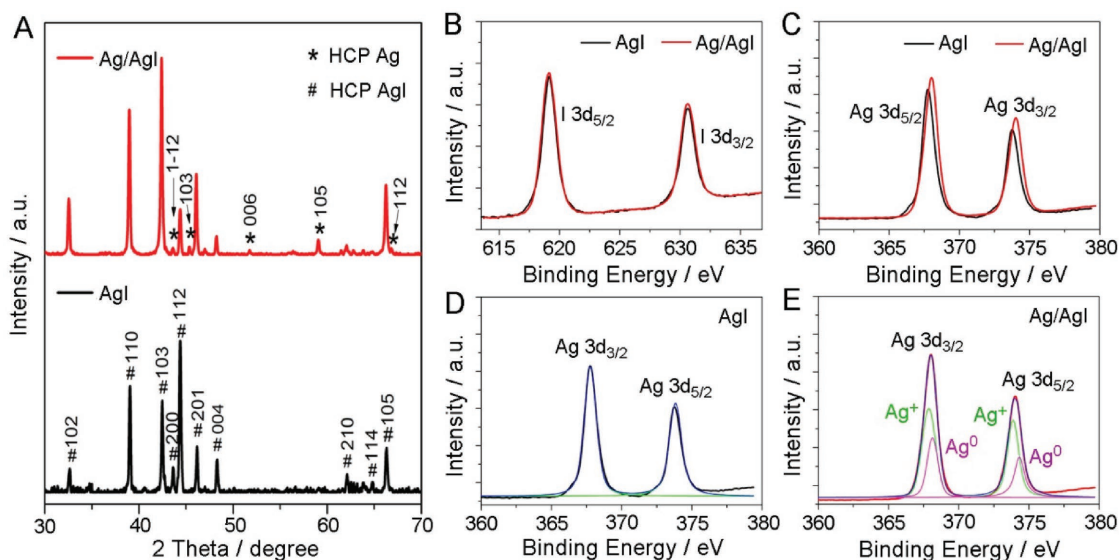


Figure 3. PXRD patterns and XPS spectra of AgI nanoplates and Ag/AgI nanoplates. A) PXRD patterns of AgI nanoplates and Ag/AgI nanoplates. Comparison for the XPS spectra of AgI nanoplates and Ag/AgI nanoplates at the lines of B) I 3d and C) Ag 3d. Gaussian function is employed to deconvolve the Ag 3d peaks of D) AgI nanoplates and E) Ag/AgI nanoplates.

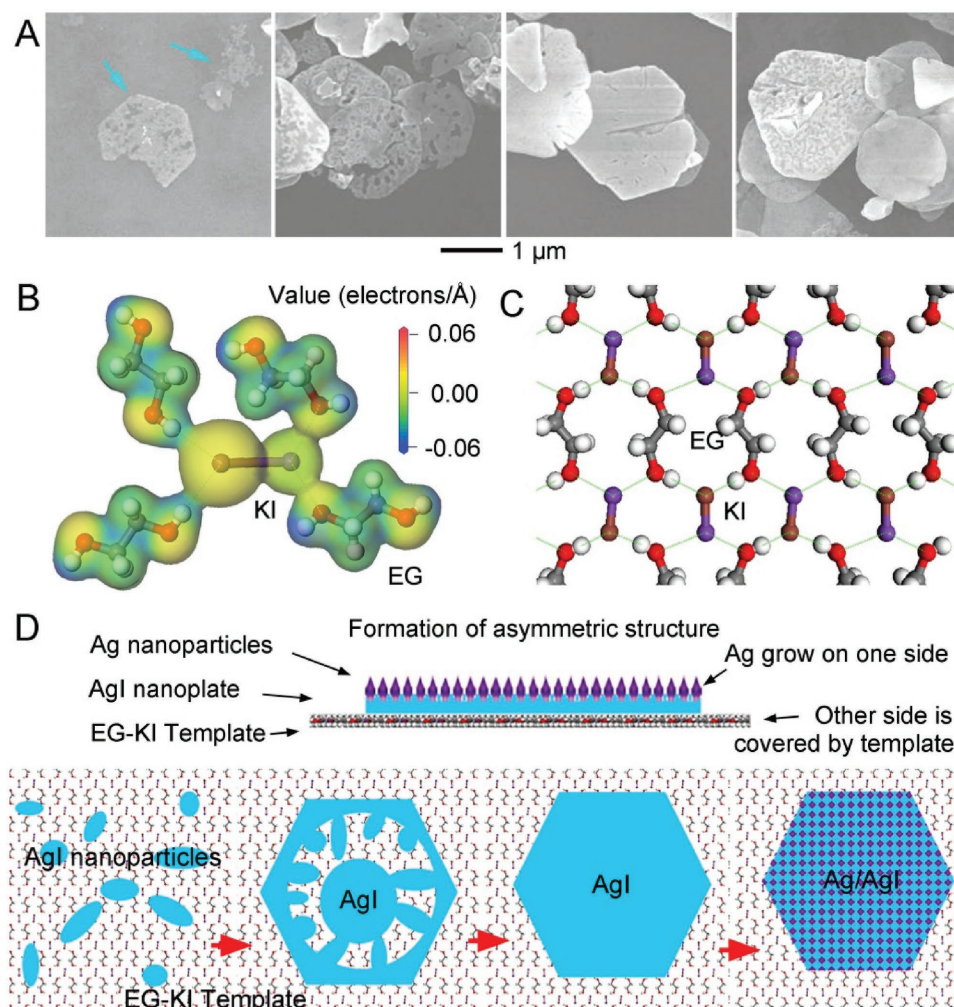


Figure 4. SEM images and schematic presentation for the formation process of the heterostructured Ag/AgI nanoplates. A) SEM images of Ag/AgI nanoplates synthesized with different reaction times: 5, 10, 30, and 90 min. B) The bond formation between EG and KI, and the correlated density distribution of electrons in the electric cloud. C) 2D frame formed by the connection of EG and KI molecules. D) Schematic image for the formation of asymmetric Ag/AgI nanoplate on the 2D EG–KI soft template.

Based on the experimental and theoretical results, the formation process of Ag/AgI nanoplates may be deduced as schematically shown in Figure 4D. In the initial stage, AgI nucleuses and NPs are produced and preferentially grow on the surface of EG–KI soft template. In the following, through a particle-mediated growth process,^[23,43] AgI NPs contact each other to form a porous nanoplate. With the addition of more AgI, the porous nanoplate transforms into a solid nanoplate with smooth surface through a coarsening process. In the final stage, I^- ions are exhausted. In this situation, if excessive Ag^+ ions still exist in the reaction system, the excessive Ag^+ ions may adsorb on one side of nanoplate and are gradually reduced by EG, thus to form a 2D nanoweb finally. However, the other side of AgI nanoplate has been covered by the EG–KI soft template (which served as a substrate for the 2D growth of AgI nanoplate, as shown in Figure 4D), hence having no growth of Ag and keeping smooth. Thus, the nonsymmetric Ag/AgI heterogeneous nanoplates are produced. In fact, it has been found that 2D soft template may play an important role

in the formation of nanoplate structures, particularly with nonsymmetric surface morphology. For example, a similar growth mode has been observed in the growth of nonsymmetric ZnO nanodisks and nanorings, in which bis(2-ethylhexyl) sulfosuccinate (NaAOT) serves as soft template for the limited growth of 2D nanostructures.^[44] Similarly, in our recent study, in the case of Au nanoplate, hexagonal Au disks with one side smooth and the other concave was formed using PEG-water soft template.^[35]

The photocatalytic activities of Ag/AgI nanoplates were evaluated by the degradation of dye molecules in water under visible-light irradiation (high pressure of mercury lamp with a UV filter).^[45,46] Figure 5A shows the absorption spectrum of the Rhodamine B (RhB) degradation in the presence of Ag/AgI nanoplates under exposure to visible light. The peak of RhB characteristic absorption at $\lambda = 554$ nm diminishes as the exposure time increases and almost disappears after 30 min. To disclose the catalytic properties of the nonsymmetric metal–semiconductor nanoplate, the samples with metal nanoparticles being symmetrically distributed on the both sides of

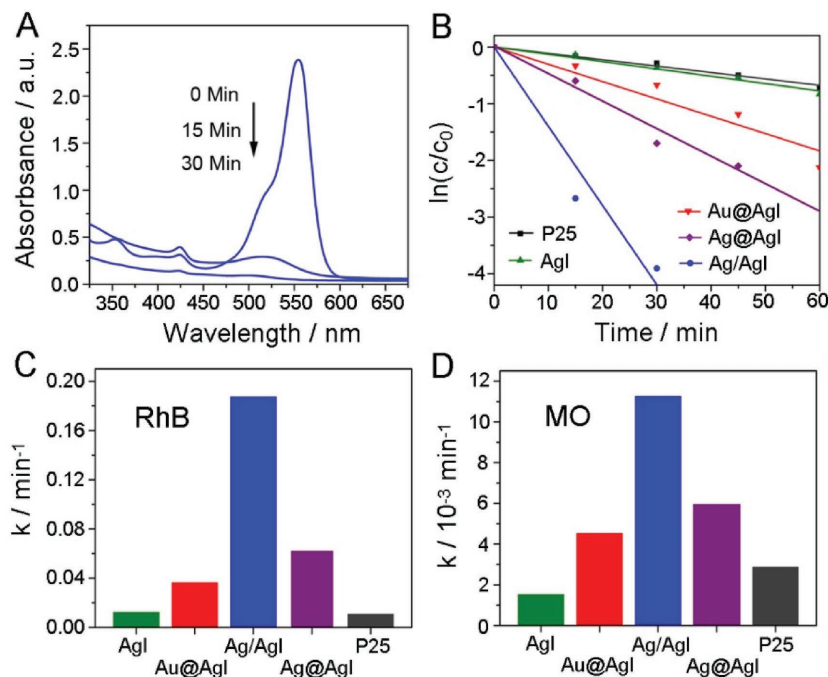


Figure 5. Photocatalytic properties of Ag/AgI nanoplates. A) Absorption spectrum of a solution of Rhodamine B (RhB) in the presence of Ag/AgI nanoplates under visible-light irradiation. B) The normalized concentration of the RhB as a function of reaction time in logarithmic scale for AgI, Au@AgI, Ag@AgI, and P25. Comparison of photocatalytic activities for the photocatalytic degradation of C) RhB and D) methyl orange (MO).

semiconductor nanoplate, including Au@AgI and Ag@AgI, are synthesized. Here, to distinguish with nonsymmetric distribution (Ag/AgI), the signal @ is used to denote both sides being decorated with metal nanoparticles (Au@AgI and Ag@AgI). As shown in Figure S11 (Supporting Information), Au nanoparticles are uniformly distributed on both sides of AgI nanoplates. Figures S12–S14 (Supporting Information) show the SEM images, EDX analysis, and PXRD patterns of Ag@AgI nanoplates, indicating that Ag nanoparticles are uniformly distributed on both sides of the AgI nanoplates. As shown in Figure S15 (Supporting Information), the UV-vis spectra of Ag/AgI, Ag@AgI, and Au@AgI possess their special extinction peaks correlated with Ag nanoparticles (at 426 nm) and Au nanoparticles (at around 590 nm).

As comparison, the photocatalytic activities of AgI nanoplates, Au@AgI nanoplates, Ag@AgI nanoplates, and commercial catalyst (TiO_2 , P25) were measured and are shown in Figure S16 (Supporting Information). Depending on the model of pseudo-first-order reaction,^[47,48] Figure 5B shows the relationships between $\ln(c/c_0)$ and irradiation time (t) for the five kinds of catalysts in the system of RhB degradation. Their correlated apparent first-order rate constants (k) are illustrated as the histograms in Figure 5C. Similarly, the photocatalytic properties of the five catalysts for the degradation of methyl orange (MO) are also measured (Figures S17 and S18) and are compared by the histograms in Figure 5D. The photocatalytic activity of pure AgI nanoplate is comparable to that of P25. An increased photocatalytic activity is obtained for the Au@AgI and Ag@AgI nanoplates, probably resulting from the improved

separation process of photogenerated electron–hole pairs by the metal–semiconductor heterostructure. Compared with Au@AgI and Ag@AgI nanoplates, the nonsymmetric Ag/AgI nanoplates show significantly further enhanced photocatalytic activities both for the degradation of RhB and MO. For the Ag@AgI and Ag/AgI nanoplates, they are totally same at material, morphology, and structure, except the nonsymmetric covering of Ag nanoparticles. Thus, the greatly improved photocatalytic property can be deduced to the assumption that the nonsymmetric metal–semiconductor heterostructure will be preferable to facilitate the separation of electron–hole pairs, as illustrated in Figure 1C.

To further deeply study the effect of nonsymmetric metal–semiconductor heterostructure on the photocatalytic properties, the samples with different loading density of Ag nanoparticles and morphology have been synthesized. In the synthesis for the Ag/AgI nanoplates, when the EG amount was increased to 24 mL, the density of Ag nanoparticles on the nonsymmetric Ag/AgI nanoplate would decrease. As shown in Figure S19 (Supporting Information), Ag nanoparticles are sparsely separated on the one side of AgI nanoplate. The photocatalytic property of sparse-Ag/AgI nanoplates for the degradation of RhB is shown in Figure S20A (Supporting Information). Compared with Ag/AgI nanoplates, the photocatalytic activity of sparse-Ag/AgI nanoplates is obviously decreased. On the other hand, when we changed the EG amount to 12 and 18 mL, the thickness of Ag/AgI nanoplates was increased from original 20 nm (Figure 2D) to 150 nm (Figure S21, Supporting Information) and around 800 nm (Figure S22, Supporting Information), respectively. The SEM images (Figures S21 and S22, Supporting Information) and UV-vis spectrum (Figure S23, Supporting Information) indicate that thick-Ag/AgI (150 nm) nanoplate and thicker-Ag/AgI nanoplate (800 nm) are nonsymmetrically covered by Ag nanoparticles on only one side of the nanoplates. The photocatalytic properties of thick-Ag/AgI nanoplates and thicker-Ag/AgI nanoplates were also measured for the degradation of RhB and are shown in Figure S24 (Supporting Information). Compared with Ag/AgI nanoplates, as shown in Figure S25 (Supporting Information), with the thickness of the nanoplates increasing, the catalytic activities greatly decrease.

Before the metal and semiconductor are attached together, usually the electronic Fermi level of semiconductor is higher than that of metal, as illustrated in Figure S26A (Supporting Information). Thus, after they are attached together, the electrons in semiconductor will transfer to metal. Because the density of carriers in semiconductor is less, the area near to the metal–semiconductor interface will exhibit positive charge after the electrons are transferred to metal. In the metal, to keep the equipotential, the transferred electrons will move to the surface of metal. At this situation, as shown in Figure S26B (Supporting Information), in the semiconductor near the interface, an

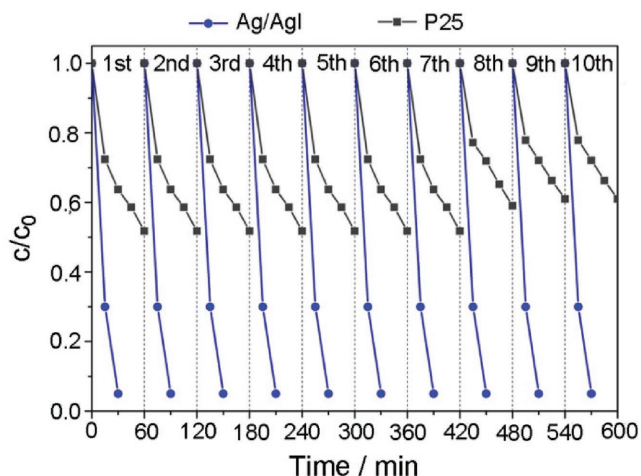


Figure 6. Comparison of photocatalytic stability of Ag/AgI and P25 for the degradation of RhB in cycling reactions.

internal electric field is built. When the metal–semiconductor heterostructure is irradiated by light, driven by the internal electric field, the photogenerated electrons will move toward the interface and the photogenerated holes will move toward the opposite direction (Figure S26C, Supporting Information). Thus, the separation of the photogenerated electrons and holes is promoted in the internal electric field. For the nonsymmetric Ag/AgI nanoplates, in the photocatalysis, the photogenerated electrons move to Ag nanoparticle and holes move to other nonmetal-covered surface. The electrons and holes can be used to catalyze the reduction reaction and oxidation reaction, respectively. If both sides of AgI nanoplate are covered by Ag nanoparticles, the photogenerated holes will be limited in the inside of AgI, which will combine with new photogenerated electrons, thus the photocatalytic property will decrease. As shown in Figure S26B (Supporting Information), the intensity of the internal electric field decreases with the increase of the distance to the interface. Thus, the function of nonsymmetric structure on promoting the separation of electrons and holes will be greatly weakened when the thickness of the nanoplate increases. Similarly, if Ag nanoparticles are sparsely loaded on the one side of AgI nanoplate, the internal electric field is only located near the Ag nanoparticles and cannot perform obvious effect on the catalytic property.

In addition to efficiency, stability and recyclability of photocatalysts are also important for applications. After the RhB molecules are completely decomposed, centrifuging the solution enables the Ag/AgI nanoplates to be easily collected to catalyze a new reaction. **Figure 6** shows the recycling photodegradation curve of Ag/AgI and commercial catalyst P25. After ten cycles, the catalytic efficiency of Ag/AgI nanoplates does not significantly decrease. Compared with the commercial photocatalyst P25, Ag/AgI shows better stability.

In summary, we have developed a facile method for the synthesis of nonsymmetric heterostructured Ag/AgI nanoplates. Under the assistance of EG–KI soft template, the shape of 2D nanoplate is formed. At the same time, the EG–KI soft template may also be used to control the in situ growth of Ag nanowires on only one side of Ag/AgI nanoplates. Compared

with heterostructured Au@AgI nanoplates that Au NPs are decorated symmetrically on both sides of nanoplate, the non-symmetrically decorated Ag/AgI nanoplates demonstrate greatly improved photocatalytic property. The nonsymmetric metal–semiconductor heterostructure is probably beneficial to facilitate the separation of photogenerated electron–hole pairs. This study may open a new way to improve the photocatalytic property of semiconductor catalysts, through further deep investigations.

Experimental Section

Synthesis of AgI and Ag/AgI Nanoplates: The AgI and heterostructured Ag/AgI nanoplates were synthesized by using simple aqueous solution, as illustrated with the schematic images in Figure S1 (Supporting Information). For the synthesis of AgI nanoplates, 9 mL of EG was taken with the addition of 0.5×10^{-3} M of silver acetate and 160 mg of PVP (K29-32) in a 20 mL vial. The solution was stirred with a magnetic stirring bar at a rate of 400 rpm for 4 min. In the second stage 1 M of KI was dissolved in deionized water, and 150 μ L was added and stirred at room temperature for 10 min until the formation of a homogeneous mixture. In the next step, the vial was put into an oil bath keeping at 140 °C for 90 min with magnetic bar at a rate of 400 rpm. Finally, the product was separated from the solution with centrifuging at 10 000 rpm for 10 min and was washed twice with the mixture of water/ethanol and once with ethanol. For the synthesis of heterostructured Ag/AgI nanoplates, the concentration of silver acetate was changed from 0.5×10^{-3} M to 2×10^{-3} M. The procedure and other conditions were kept same with the synthesis of AgI nanoplates.

Synthesis of Au@AgI (AgI Nanoplates Decorated with Au Nanoparticles on Both Sides): An amount of 122 mg above synthesized AgI nanoplates was dispersed in 50 mL DI water through ultrasonication for 2 min. Then 5 mL of the AgI solution was taken and put into a bottle, which was kept at 0 °C through ice-water bath. An amount of 10 mg of L-ascorbic acid (AA) was added into the bottle followed by drop wise inputting of 100 μ L of 5×10^{-3} M HAuCl₄ aqueous solution under the stirring at the velocity of 400 rpm. The reaction was carried out at 0 °C for 1 h. The final product was separated by centrifuging at 10 000 rpm for 5 min, and washed two times with the mixture of DI water and ethanol to remove the remaining AA and HAuCl₄.

Synthesis of Ag@AgI (AgI Nanoplates Decorated with Ag Nanoparticles on Both Sides): An amount of 122 mg above synthesized AgI nanoplates was dispersed in 50 mL DI water through ultrasonication for 2 min. Then 5 mL was taken and put into a bottle, which was kept at 0 °C through ice-water bath. An amount of 200 μ L of 10×10^{-3} M AgNO₃ aqueous solution was added drop wise. The reaction was carried out at 0 °C for 90 min. The final product was separated by centrifuging at 10 000 rpm for 5 min, and washed two times with the mixture of DI water and ethanol to remove the remaining AgNO₃.

Characterizations: The morphologies of the prepared products (AgI, Ag/AgI, Au@AgI, and Ag@AgI) were characterized with field emission SEM (JEOL JSM-7000F) and TEM (JEOL JEM-3010). EDX analysis was performed with an Oxford INCA detector installed on the SEM. The PXRD patterns were recorded using a BRUKER D8 ADVANCE X-ray diffractometer with a Cu K α X-ray source ($\lambda = 1.5405$ Å).

Measurement of Photocatalytic Properties: The as prepared catalysts (10 mg, AgI, Ag/AgI, Au@AgI, Ag@AgI or P25) and 0.5 mg of RhB or MO were added in a flask containing of 50 mL DI water. The solution was stirred at ultrasonication for 20 min under dark condition. Then, the photocatalytic test was performed under a 300 W high-pressure mercury lamp with a 420 nm cutoff filter as the light source. Analytical samples with certain reaction times were taken out from the reaction suspension and centrifuged at 10 000 rpm for 2 min to remove the catalyst. The transparent solution was analyzed by a UV–vis spectrometer, and the absorbance was measured at wavelengths of 526 and 470 nm, corresponding to the maximum absorption wavelengths of RhB and MO, respectively.

Supporting Information

Supporting Information is available from the Wiley Online Library or from the author.

Acknowledgements

This work was supported by the National Natural Science Foundation of China (Grant No. 21675122), the Natural Science Foundation of Shaanxi Province (Grant Nos. 2017JM5072 and 2017NY-114), and the Fundamental Research Funds for the Central Universities (Grant No. xjj2017102).

Conflict of Interest

The authors declare no conflict of interest.

Keywords

metal–semiconductor heterostructures, nanoplates, nonsymmetric structures, photocatalysis

Received: August 26, 2017
Revised: November 22, 2017
Published online:

- [1] C. L. Yu, G. Li, S. Kumar, K. Yang, R. C. Jin, *Adv. Mater.* **2014**, 26, 892.
- [2] Y. D. Hou, A. B. Laursen, J. S. Zhang, G. G. Zhang, Y. S. Zhu, X. C. Wang, S. Dahl, I. Chorkendorff, *Angew. Chem., Int. Ed.* **2013**, 52, 3621.
- [3] T. W. Kim, K. S. Choi, *Science* **2014**, 343, 990.
- [4] H. L. Wang, L. S. Zhang, Z. G. Chen, J. Q. Hu, S. J. Li, Z. H. Wang, J. S. Liu, X. C. Wang, *Chem. Soc. Rev.* **2014**, 43, 5234.
- [5] H. Tong, S. X. Ouyang, Y. P. Bi, N. Umezawa, M. Oshikiri, J. H. Ye, *Adv. Mater.* **2012**, 24, 229.
- [6] R. Marschall, *Adv. Funct. Mater.* **2014**, 24, 2421.
- [7] S. J. A. Moniz, S. A. Shevlin, D. J. Martin, Z. X. Guo, J. W. Tang, *Energy Environ. Sci.* **2015**, 8, 731.
- [8] H. J. Wang, F. Q. Sun, Y. Zhang, L. S. Li, H. Y. Chen, Q. S. Wu, J. C. Yu, *J. Mater. Chem.* **2010**, 20, 5641.
- [9] W. Wu, S. F. Zhang, J. Zhou, X. H. Xiao, F. Ren, C. Z. Jiang, *Chem.—Eur. J.* **2011**, 17, 9708.
- [10] J. Kundu, D. Pradhan, *ACS Appl. Mater. Interfaces* **2014**, 6, 1823.
- [11] H. Wang, X. F. Lang, R. Hao, L. Guo, J. H. Li, L. H. Wang, X. D. Han, *Nano Energy* **2016**, 19, 8.
- [12] J. Y. Liu, T. Luo, T. S. Mouli, F. L. Meng, B. Sun, M. Q. Li, J. H. Liu, *Chem. Commun.* **2010**, 46, 472.
- [13] Y. X. Tang, Z. L. Jiang, G. C. Xing, A. R. Li, P. D. Kanhere, Y. Y. Zhang, T. C. Sum, S. Z. Li, X. D. Chen, Z. L. Dong, Z. Chen, *Adv. Funct. Mater.* **2013**, 23, 2932.
- [14] P. Li, Z. Wei, T. Wu, Q. Peng, Y. D. Li, *J. Am. Chem. Soc.* **2011**, 133, 5660.
- [15] M. T. Niu, F. Huang, L. F. Cui, P. Huang, Y. L. Yu, Y. S. Wang, *ACS Nano* **2010**, 4, 681.
- [16] A. Kudo, Y. Miseki, *Chem. Soc. Rev.* **2009**, 38, 253.
- [17] A. Kubacka, M. Fernandez-Garcia, G. Colon, *Chem. Rev.* **2012**, 112, 1555.
- [18] H. Tada, T. Kiyonaga, S. Naya, *Chem. Soc. Rev.* **2009**, 38, 1849.
- [19] R. Abe, H. Takami, N. Murakami, B. Ohtani, *J. Am. Chem. Soc.* **2008**, 130, 7780.
- [20] A. O. Ibhadon, P. Fitzpatrick, *Catalysts* **2013**, 3, 189.
- [21] A. A. Herzog, C. J. Kiely, A. F. Carley, P. Landon, G. J. Hutchings, *Science* **2008**, 321, 1331.
- [22] G. C. Xi, J. H. Ye, Q. Ma, N. Su, H. Bai, C. Wang, *J. Am. Chem. Soc.* **2012**, 134, 6508.
- [23] H. J. You, F. L. Zhang, Z. Liu, J. X. Fang, *ACS Catal.* **2014**, 4, 2829.
- [24] C. H. An, S. N. Peng, Y. G. Sun, *Adv. Mater.* **2010**, 22, 2570.
- [25] P. Wang, B. B. Huang, X. Y. Qin, X. Y. Zhang, Y. Dai, J. Y. Wei, M. H. Whangbo, *Angew. Chem., Int. Ed.* **2008**, 47, 7931.
- [26] Y. Y. Fan, W. G. Ma, D. X. Han, S. Y. Gan, X. D. Dong, L. Niu, *Adv. Mater.* **2015**, 27, 3767.
- [27] S. K. Wu, X. P. Shen, Z. Y. Ji, G. X. Zhu, C. J. Chen, K. M. Chen, R. Bu, L. M. Yang, *CrystEngComm* **2015**, 17, 2517.
- [28] W. S. Choi, G. Y. Byun, T. S. Bae, H. J. Lee, *ACS Appl. Mater. Interfaces* **2013**, 5, 11225.
- [29] Y. Yang, Y. Zhao, Y. K. Yan, Y. L. Wang, C. Y. Guo, J. S. Zhang, *J. Phys. Chem. B* **2015**, 119, 14807.
- [30] P. Wang, B. B. Huang, X. Y. Zhang, X. Y. Qin, H. Jin, Y. Dai, Z. Y. Wang, J. Y. Wei, J. Zhan, S. Y. Wang, J. P. Wang, M. H. Whangbo, *Chem.—Eur. J.* **2009**, 15, 1821.
- [31] S. K. Wu, X. P. Shen, Z. Y. Ji, G. X. Zhu, H. Zhou, H. M. Zang, T. F. Yu, C. J. Chen, C. S. Song, L. H. Feng, M. Zhao, K. M. Chen, *J. Alloys Compd.* **2017**, 693, 132.
- [32] M. S. Zhu, P. L. Chen, M. H. Liu, *ACS Nano* **2011**, 5, 4529.
- [33] J. Jiang, H. Li, L. Z. Zhang, *Chem.—Eur. J.* **2012**, 18, 6360.
- [34] M. S. Zhu, P. L. Chen, M. H. Liu, *J. Mater. Chem.* **2011**, 21, 16413.
- [35] J. X. Fang, J. Li, C. F. Tian, Q. Q. Gao, X. J. Wang, N. Y. Gao, X. L. Wen, C. S. Ma, H. J. You, Z. L. Yang, Q. H. Xu, Q. H. Xiong, Z. Y. Li, *NPG Asia Mater.* **2016**, 8, e323.
- [36] M. Sigalas, D. A. Papaconstantopoulos, N. C. Bacalis, *Phys. Rev. B* **1992**, 45, 5777.
- [37] F. Jona, P. M. Marcus, *J. Phys.: Condens. Matter* **2004**, 16, 5199.
- [38] X. H. Liu, J. Luo, J. Zhu, *Nano Lett.* **2006**, 6, 408.
- [39] H. Y. Liang, H. X. Yang, W. Z. Wang, J. Q. Li, H. X. Xu, *J. Am. Chem. Soc.* **2009**, 131, 6068.
- [40] G. H. Jeong, M. Kim, Y. W. Lee, W. Choi, W. T. Oh, Q. H. Park, S. W. Han, *J. Am. Chem. Soc.* **2009**, 131, 1672.
- [41] H. J. You, X. T. Liu, H. Z. Liu, J. X. Fang, *CrystEngComm* **2016**, 18, 3934.
- [42] H. J. You, W. J. Wang, S. C. Yang, *ACS Appl. Mater. Interfaces* **2014**, 6, 19035.
- [43] H. J. You, J. X. Fang, *Nano Today* **2016**, 11, 145.
- [44] F. Li, Y. Ding, P. X. X. Gao, X. Q. Xin, Z. L. Wang, *Angew. Chem., Int. Ed.* **2004**, 43, 5238; *Angew. Chem.* **2004**, 116, 5350.
- [45] Z. Y. Lin, J. Xiao, J. H. Yan, P. Liu, L. H. Li, G. W. Yang, *J. Mater. Chem. A* **2015**, 3, 7649.
- [46] H. J. You, R. Liu, C. C. Liang, S. C. Yang, F. Wang, X. G. Lu, B. J. Ding, *J. Mater. Chem. A* **2013**, 1, 4097.
- [47] T. B. Devi, M. Ahmaruzzaman, S. Begum, *New J. Chem.* **2016**, 40, 1497.
- [48] Y. H. Liang, H. Wang, L. Liu, P. F. Wu, W. Q. Cui, J. McEvoy, Z. S. Zhang, *J. Mater. Sci.* **2015**, 50, 6935.